Materials Science and Engineering A 528 (2011) 8277–8285

Contents lists available at ScienceDirect

Materials Science and Engineering A

journal homepage: www.elsevier.com/locate/msea

Study of the hot deformation behaviour in Ti–5Al–5Mo–5V–3Cr–1Zr

F. Warchomicka [a,*], C. Poletti [b], M. Stockinger [c]

[a] Vienna University of Technology, Karlsplatz 13/E308, A-1040 Vienna, Austria
[b] Graz University of Technology, Kopernikusgasse 24/I, A-8010 Graz, Austria
[c] Böhler Schmiedetechnik GmbH & Co KG, Mariazellerstraße 25, A-8605 Kapfenberg, Austria

ARTICLE INFO

Article history:
Received 11 October 2010
Received in revised form 28 July 2011
Accepted 29 July 2011
Available online 4 August 2011

Keywords:
EBSD
Electron microscopy
Titanium alloys
Thermomechanical processing
Recrystallization

ABSTRACT

Structural applications of near beta titanium alloys are gradually increasing in the aerospace industry because of their high specific mechanical properties and good corrosion resistance. Furthermore, a wide range of microstructures can be obtained by thermomechanical processes. This work determines by the use of EBSD technique the mechanism of restoration active in the near beta titanium alloy Ti–5Al–5Mo–5V–3Cr–1Zr for deformations in both α + β and β field near to the β transus temperature (T_β = 803 °C). Hot compression tests are carried out up to 0.7 true strain by means of a Gleeble® 1500 machine at strain rates of 0.01, 0.1 and 1 s^{-1}. Dynamic recovery of β phase and rotation of the α grains take place predominantly in the α + β field. Further deformation produces continuous dynamic recrystallization of the β phase influenced by the strain rate. Dynamic recovery is observed during deformation above the T_β, where the misorientation is increasing towards the grain boundaries forming new small grains with a substructure at high strain rates and larger deformation. The stress exponent and the apparent activation energy for the sinh constitutive equations are determined and the microstructural features are correlated with the Zener–Hollomon parameter.

1. Introduction

The evolution of engineering materials is giving us opportunities for innovation in mechanical design by the substitution of conventional materials in different application fields [1]. Titanium alloys are very attractive not only for aerospace application but also for process engineering, automotive, medical and sport applications owing to the high specific bending stiffness and strength, combined with corrosion and creep resistance [2]. The use of β and near β titanium alloys is gradually increasing for structural applications in the aerospace industry [3,4]. They exhibit a relatively good workability due to the low β transus temperature (T_β) compared to typical α + β alloys. Strengthening by grain refinement and precipitation of fine α phase yields similar strength levels as low alloyed and even some stainless steels.

Thermomechanical processing techniques are necessary not only for shaping, but also for adjusting the mechanical properties obtaining an appropriate microstructure. Previous works of near β titanium alloys have shown that isothermal or near-isothermal hot working in the subtransus region provokes flow softening at high strain rates by adiabatic heating provoking a change in the texture of the α phase [5]. The apparent energy of activation of the hot deformation was determined to be in the range of 300–700 kJ/mol, values which are significantly higher than the self-diffusion of the β phase in pure titanium (135–153 kJ/mol) [6–8]. Thus, the active mechanism of restoration is very sensitive to changes of the working temperature. Superplasticity was observed for Ti–10V–2Fe–3Al (Ti-10-2-3) with a globular starting microstructure at strain rates below 0.1 s^{-1} [9–11]. Furuhara et al. [11], observed that dynamic discontinuous and continuous recrystallization can take place in the β phase for large deformations in the α + β field at strain rates up to 4.2×10^{-2} s^{-1}. It was shown that both recrystallization mechanisms depend on the amount of α phase present during deformation. Continuous dynamic recrystallization in the β phase during torsion experiments was also determined for beta Cez alloy [14]. Dynamic recovery in β phase was also suggested for the metastable Ti-10-2-3 titanium alloy under isothermal forging, while the α grains globularizes and spherodizes by diffusion [15,16]. Ti-5-5-5-3 alloy showed insignificant dependence of the globular α grain area with strain and strain rate, and a predominant steady state flow behaviour during isothermal compression [17]. An increment of the flow softening with increasing the strain rate and the volume of α phase was determined for Timetal 555 [18]. Jones et al. [17] concluded that dynamic recovery is the main mechanism of restoration of the β phase because the calculated activation energy value is similar to that of the self-diffusion of pure β-Ti. Most of the publications reported dynamic recovery as the dominant restoration mechanism in the β region with apparent activation energy close to the self-diffusion in β-Ti. Dynamic recrystallization was also observed by optical microscopy [18–20].

* Corresponding author. Tel.: +43 1 58801 30820; fax: +43 1 58801 30899.
E-mail address: fwarchom@pop.tuwien.ac.at (F. Warchomicka).

0921-5093/$ – see front matter © 2011 Elsevier B.V. All rights reserved.
doi:10.1016/j.msea.2011.07.068

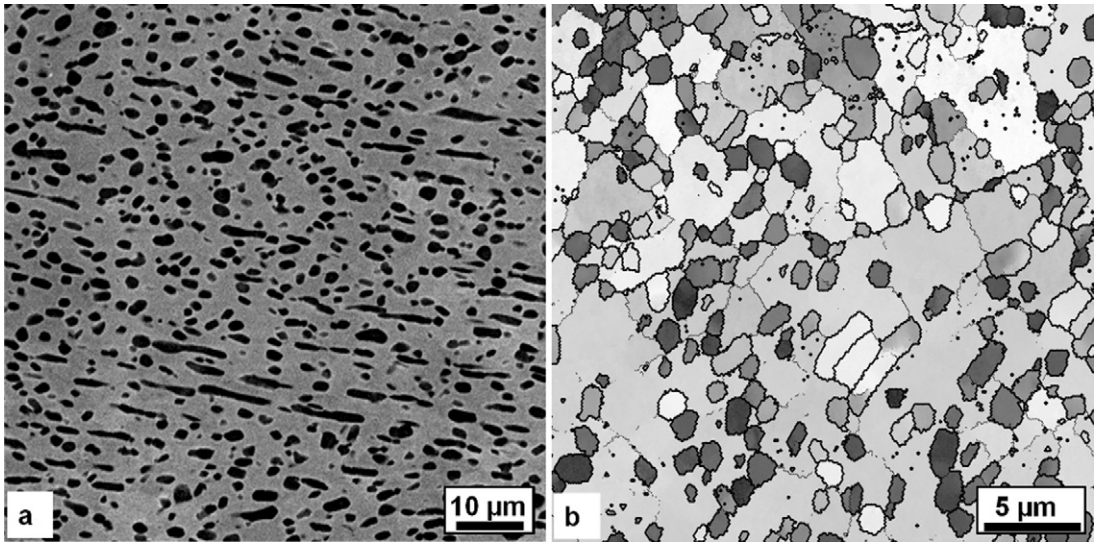

Fig. 1. Ti55531 in the as received material: (a) SEM BSE image where the α phase is dark and the β phase is bright. (b) EBSD orientation map (ND–RD plane) identifying subgrains (narrow lines) and grains boundaries (thicker lines) in the α and β phase.

This work investigates the microstructural evolution of a pre-forged and annealed Ti–5Al–5Mo–5V–3Cr–1Zr (Ti55531) by hot compression above and below T_β to optimize the forging process. The particular interest on this alloy is the lower T_β in comparison with similar alloys (i.e. Ti-5-5-5-3, Timetal 555, VT 22), a fact that is attractive for the forging industry. Preliminary results [21] showed an elongation of the α grains with refinement of β subgrains or grains when increasing the strain rate to 1 s^{-1}. For deformations in the β region, the formation of a necklace structure was observed at the borders of β grains which was related to dynamic recrystallization. The use of typical metallography techniques was not sufficient to differentiate the β subgrains from the grains and thus to determine more accurately the restoration mechanism active during the deformation.

This work analyses the microstructure evolution related to the local deformation parameters in the compression specimens and their flow behaviour. The restoration mechanism taking place during hot deformation is deduced from metallography using electron backscatter diffraction (EBSD).

2. Experimental

The chemical composition of the investigated Ti55531 in wt% is: 5.04V, 5.51Al, 5.01Mo, 2.85Cr, 0.32Fe, 1.125Zr, 0.0655O, 0.0045C, 0.0085N and Ti (balance). The T_β determined by the supplier and corroborated by metallographic observations for this alloy is 803 °C [22]. The double melt material has been pre-forged (by cogging) to billet dimensions with a final step in the α + β field followed by an annealing treatment below beta transus temperature. Cylindrical specimens of 15 mm length and 10 mm diameter were machined with the axis perpendicular to the pre-forging direction of the billet. After deformation, the specimens were cut parallel to the load axis. The longitudinal section was mechanically ground and polished prior to observation in a scanning electron microscope (SEM) set in the backscatter electron mode (BSE). The α could be distinguished because it is shown darker than the β phase due to its lower Mo content. Around 20 pictures were taken each of each specimen from its border to its centre along the maximum diameter. The quantitative analysis of the pictures was carried out using the software Axio Vs40 v4.4 to determine the α content, the size (area) and aspect ratio (as Feret minimum length/Feret maximum length) of the α grains. At least 500 α grains were analyzed for each condition.

EBSD scans were carried out with the sample tilted 70°, applying an accelerating voltage of 20 kV, a spot size of around 4 nm and at a working distance of 10 mm. An increment step of 0.1 μm was used for samples with α grains and of 0.3–5 μm for samples thermomechanically treated above T_β. The β phase could be retained at room temperature by fast cooling. The confidence index (CI) average values of each measurement (raw data) were higher than 0.3 and the misorientation data represented adjacent points.

Hot compression tests were carried out using a Gleeble® 1500 machine with servo hydraulic system at strain rates of 0.01, 0.1 and 1 s^{-1} in the temperature range of $T_\beta \pm 40$ °C, up to global true strains of 0.1, 0.2 and 0.7. The specimens were heated to the compression temperature at 5 K/s and held at least 900 s. The temperature was controlled by a K type thermocouple welded in the middle of the specimens. Three additional thermocouples were used to record the temperature gradient along the sample. The deformation was controlled by the stroke and the strain was measured by means of a transverse strain gauge located at the middle of each specimen to eliminate any effect of the longitudinal gradient of temperature and the friction at the anvils (barrelling) on the flow curves. The tests were carried out in argon atmosphere in order to prevent the formation of α case, and "sandwiches" of a graphite foil, colloidal graphite and a Mo foil were used between the anvils and the sample to reduce the temperature gradient along the specimen up to 20–40 °C. The finite elements methods (FEM) simulations were carried out for the local deformation parameters using DEFORM™2D adjusting the friction factor to the geometry obtained after deformation. The calculated local strain and strain rate in the specimens were correlated to the observed microstructure. This method was successfully applied for the interpretation of processing maps in [23].

3. Results

3.1. Microstructure before hot deformation

The as received material Ti55531 (Fig. 1) presented mostly a globular microstructure of the α phase as result of the pre-forging process and the heat treatments. The initial content of alpha is about 30%. There are indications of β subgrains in the as received billet as shown by the EBSD image.

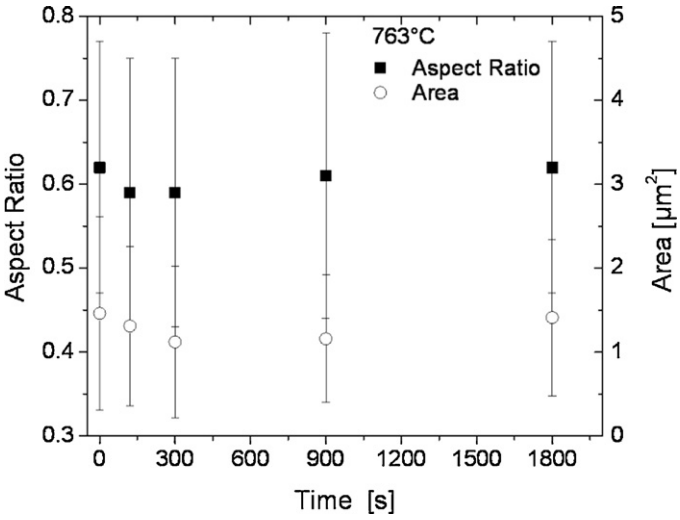

Fig. 2. Area and aspect ratio evolution of α grains after isothermal heat treatment at 763 °C.

The content of α phase decreased with the holding time during isothermal heat treatment in the α + β field till 300 s, where the α content was of 13 ± 2% and 8 ± 1% at 763 and 783 °C, respectively. The area and the shape of the α grains, illustrated by the aspect ratio, do not change significantly (Fig. 2) in the first 30 min although Ostwald ripening effect was determined by the change of the size with longer exposition times in [24].

The value of β transus temperature (803 °C) was confirmed in our alloy by using metallographic observations as shown in Fig. 3. Similar chemical composition alloys were reported with T_β values between 850 and 870°C [17,25,26] with higher concentration of oxygen (α-stabilizer) and no presence of Zr (β-stabilizer). The low amount of oxygen and other interstitials should be the main reason of the low β transus temperature compared to the literature value for similar alloys. Zr could help also to decrease the β transus temperature although 1 wt% should not be enough.

The α phase was completely transformed into β after 180 s at the tested temperatures above 803 °C. Fully static recrystallization of the β phase was achieved after 900 s at 843 °C, with a mean β grain diameter of 79 ± 3 μm. Fig. 4 shows EBSD measurements of the evolution of the β grains with the time at 843 °C.

3.2. Compression tests

3.2.1. Flow behaviour

Fig. 5 depicts the flow curves of Ti55531 at different temperatures and strain rates. The curves at 0.1 and 1 s^{-1} below the T_β exhibit softening after an initial sharp peak and steady state at 0.01 s^{-1}. The deformation carried out above the β transus temperature resulted in flow steady state for all the strain rates after an initial peak flow stress. The flow curves at 803 °C exhibit similar behaviour than that observed above T_β. An increment of the

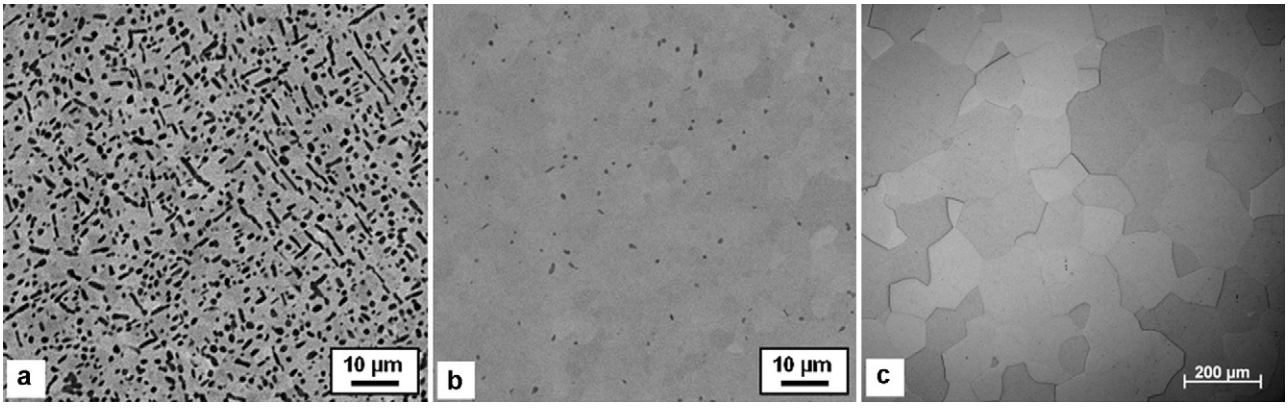

Fig. 3. Microstructure evolution after isothermal heat treatment at 803 °C after (a) 0 s, (b) 900 s and (c) 7200 s.

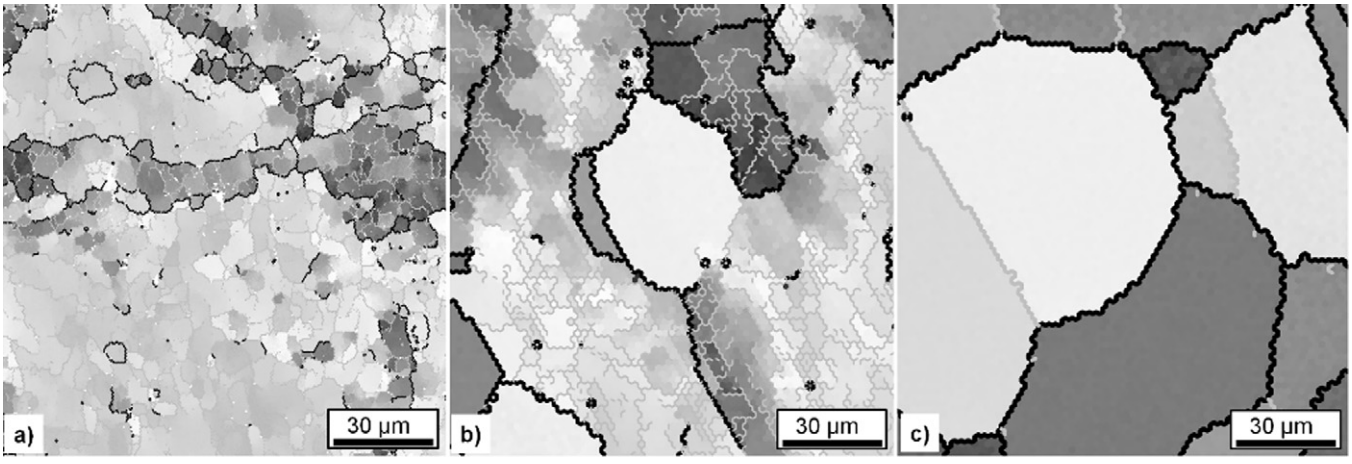

Fig. 4. EBSD orientation map (ND–RD plane) of heat treated samples above the β transus temperature (843 °C) after (a) 60 s, (b) 180 s and (c) 900 s. Subgrain and grain boundaries can be observed in grey and in bold lines, respectively.

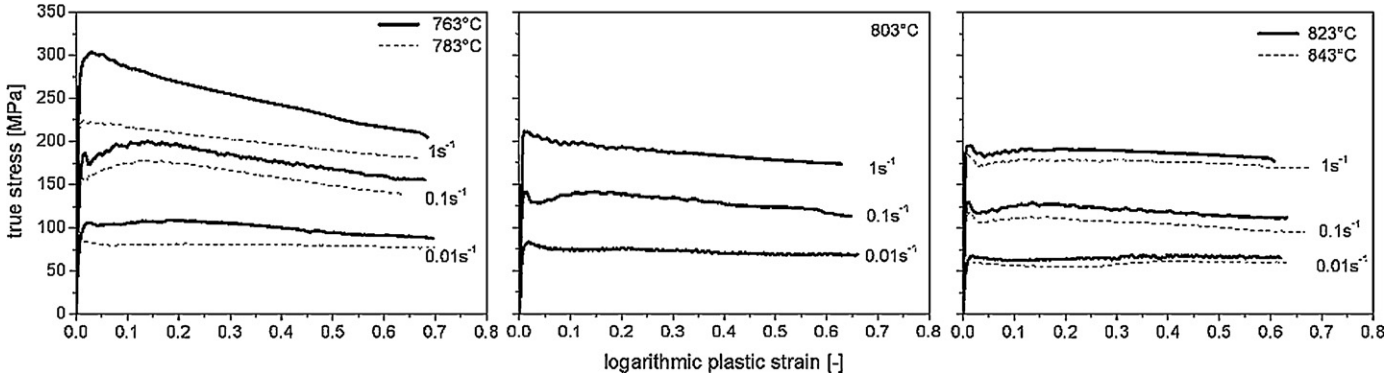

Fig. 5. Flow curves behaviour for different temperatures and strain rates.

temperature of about 30 °C during deformations at 1 s^{-1} was measured with the thermocouple at the surface of the sample. Higher stress values than Ti-5-5-5-3 alloy [17] and Timetal 555[18] should be related to the solid solution strengthening contribution of Zr due to the uniformity content in both α and β phases as observed in the Ti–6Al–2Sn–4Zr–6Mo alloy [27].

3.2.2. Microstructural behaviour after deformation

The microstructure evolution during deformation in the α + β field is shown in Fig. 6. The α grains do not show significant change in the size but they take a preferential orientation almost perpendicular to the load axis for all the strain rates and strains greater than 0.2. This effect was also observed at higher strains in double truncated cone samples of Ti-5-5-5-3 in [17]. The mean size of the α grains as well as the mean aspect ratio decrease slightly with strain for all the deformation parameters (Fig. 7a and b, respectively). There is no perceptible influence of the strain rate on the α grains as was also reported in Ti-5-5-5-3 [17]. The β subgrain size was influenced by the temperature and strain rate. The formation of β grains with similar size to the subgrains was observed by EBSD images at the prior β grain boundaries (Fig. 8c). Smaller β subgrains were observed at a higher strain rate compared to the samples deformed at 0.01 s^{-1} (Fig. 8d).

Formation of subgrain structure was observed after deformation at 843 °C for all the strain rates as shown in Fig. 9. The deformation at high strain rates (>1), produced a heterogeneous distribution of misorientations and the formation of new small grains at the original β grain boundary.

3.2.3. Constitutive equations

The dependence of the flow stress (σ) with the strain rate ($\dot{\varepsilon}$) and deformation temperature can be related using the constitutive

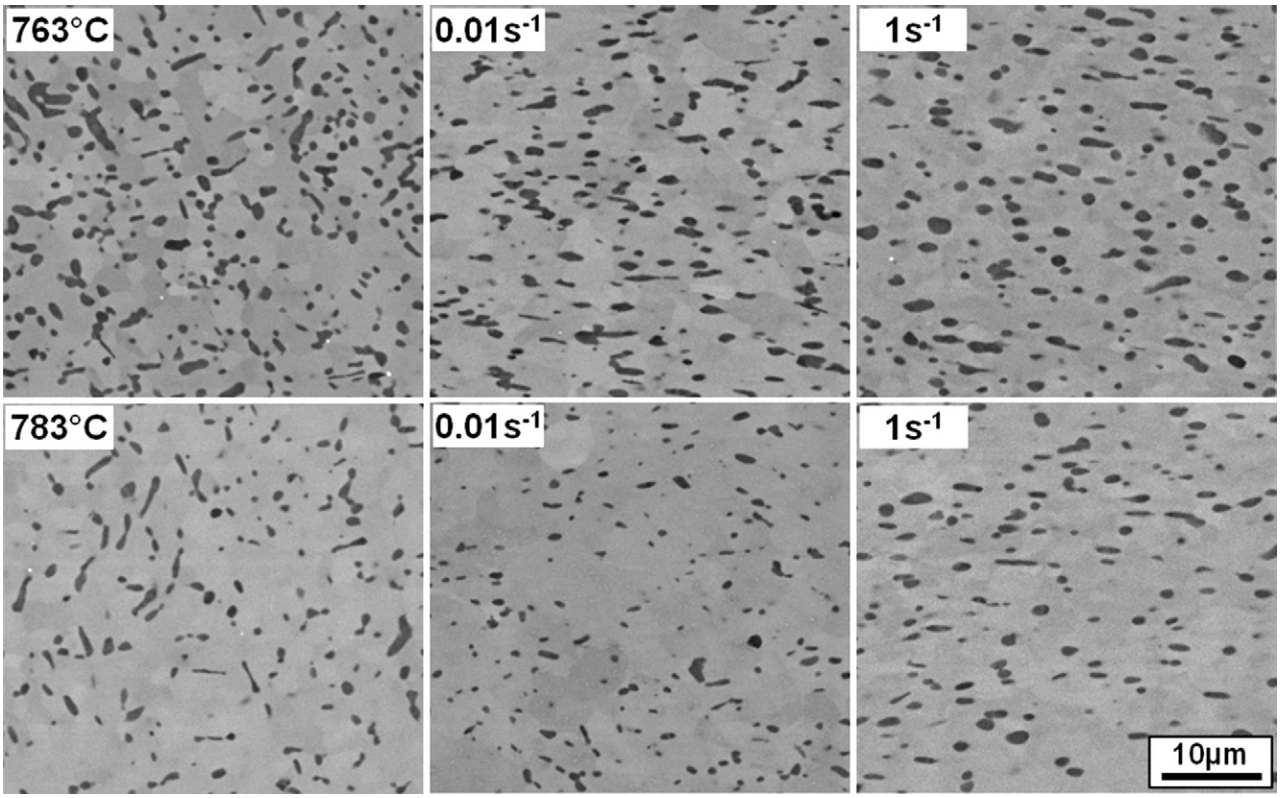

Fig. 6. SEM images of samples treated at 763 °C and 783 °C before deformation (left) and after deformation at 0.01 and 1 s^{-1} to a local strain of 0.7. Compression axis is vertical.

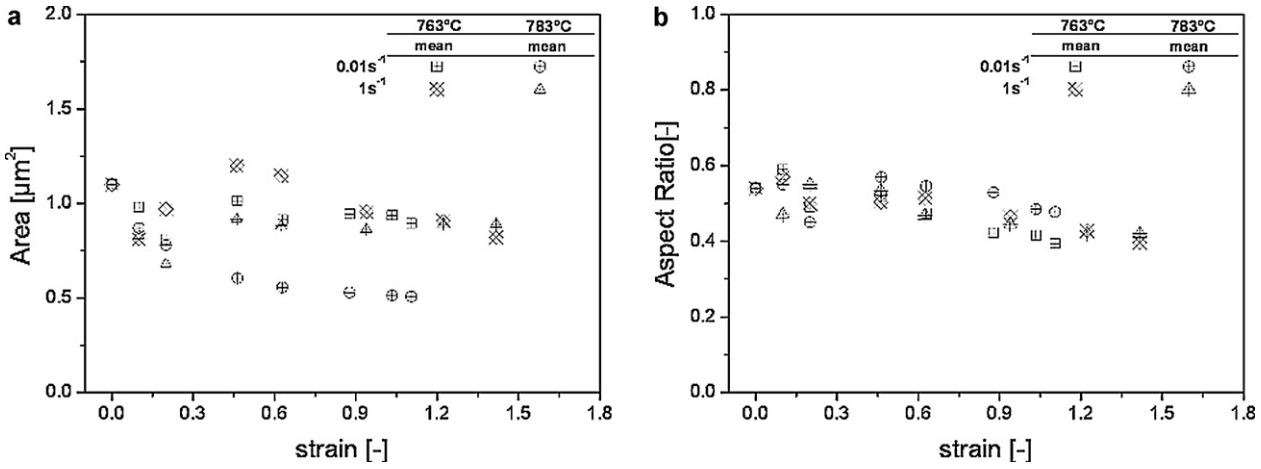

Fig. 7. Mean values of the microstructural features of the α grains with the deformation parameters: (a) area and (b) aspect ratio.

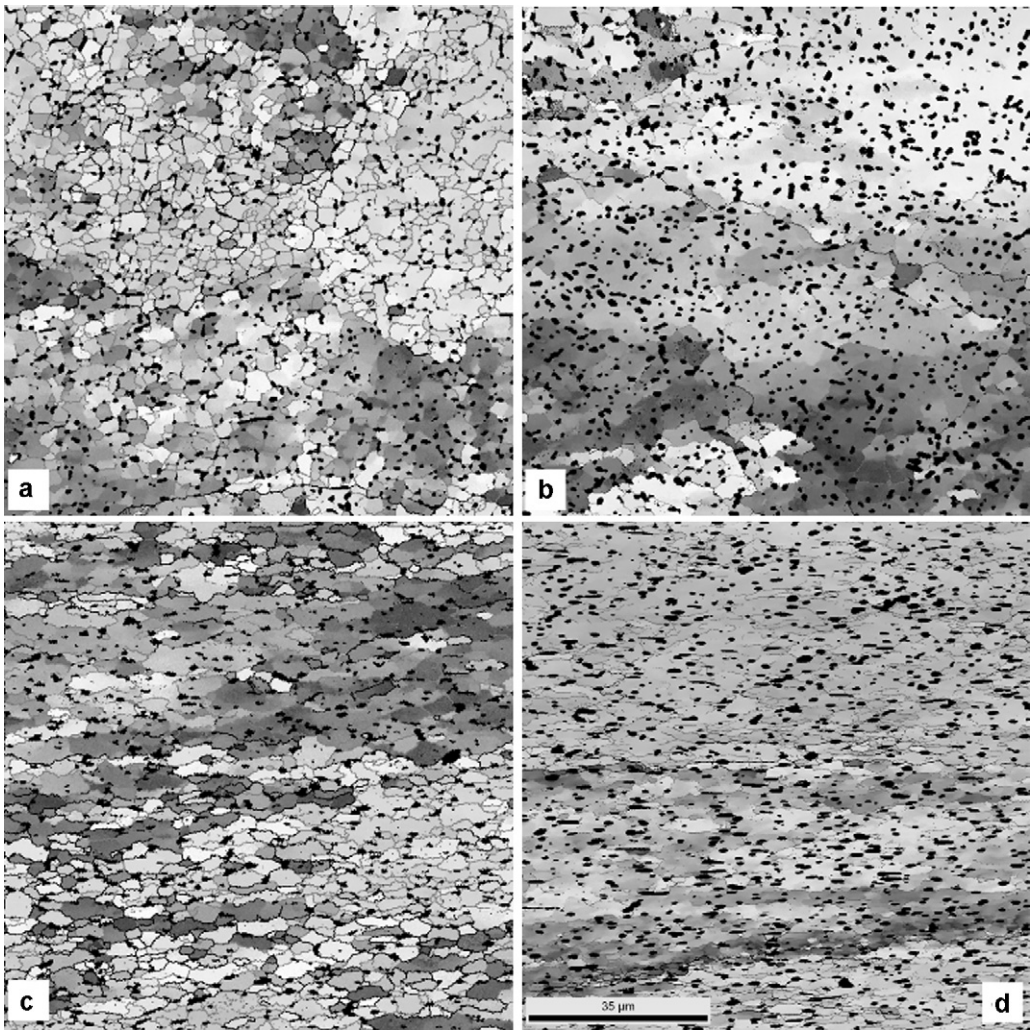

Fig. 8. EBSD orientation map (ND–RD plane) of samples treated at 763 °C: (a) non deformed, (b and c) 0.2 and 0.7 of strain at $0.01 s^{-1}$, respectively; (d) 0.7 of strain at $1 s^{-1}$. Dark grain boundaries correspond to high angle boundary (15–180°). Subgrain boundaries (less than 15°) are represented with grey lines. The α grains (black) are embedded in the β phase. Compression axis is vertical.

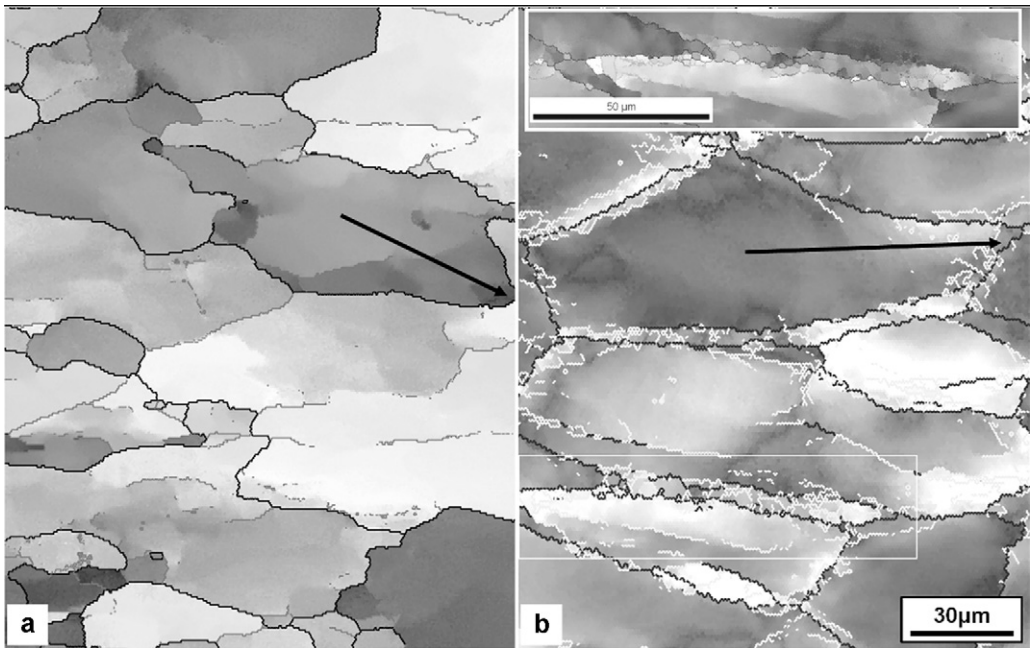

Fig. 9. EBSD orientation map (ND–RD plane) of samples deformed at 843 °C up to 0.7: (a) 0.01 s^{-1} and (b) 1 s^{-1} with detail of the β grain boundary. Dark grain boundaries correspond to high angle boundary (15–180°). Subgrain boundaries (less than 15°) are represented with grey lines. Compression axis is vertical. Arrows indicate the location of the misorientation profiles illustrated in Fig. 13.

equation proposed by Sellars and Tegart [28] that includes the creep power law and the equation for higher stresses [29]:

$$\dot{\varepsilon} = A[\sinh(c\sigma)]^n \exp\left(\frac{-Q}{RT}\right) \quad (1)$$

where Q is the apparent activation energy of deformation, R is the gas constant, T is the deformation temperature, A and c are the material constants and n is the stress exponent. Rewriting the hot working equation the following is obtained:

$$Z = \dot{\varepsilon} \exp\left(\frac{Q}{RT}\right) = A[\sinh(c\sigma)]^n \quad (2)$$

where Z is the Zener–Hollomon parameter. The values of Q and n obtained are indicators of the deformation mechanisms which should be corroborated by microstructure observations.

The activation energy of the process is determined from Eq. (2):

$$\ln Z = \ln \dot{\varepsilon} + \frac{Q}{RT} = \ln A + n \ln[\sinh(c\sigma)] \quad (3)$$

It is transformed into:

$$\ln[\sinh(c\sigma)] = \frac{(\ln \dot{\varepsilon} - \ln A)}{n} + \frac{Q}{nRT} \quad (4)$$

In Eq. (4), c is the stress multiplier that provides an adjustable constant to bring $c\sigma$ into the correct range in order to generate parallel lines for constant temperatures in $\ln \dot{\varepsilon}$ versus ln [sinh ($c\sigma$)] plots. As c increases, n decreases. The activation energy can be estimated by the slope of the Arrhenius plot ln [sinh ($c\sigma$)] versus $1/T$. These assumptions are based on the negligible changes of the microstructure of the constituent phases during deformation.

In the case of Ti55531, the microstructure of α + β and β was thus modelled using two linear ranges from which the activation energy was separately calculated for the two regions. However, it should be taken into account that within each phase region, the β subgrain size varied with temperature and strain rate. The grain shape itself is known to change when compressed as well as the amount of phases when the β transus is approached. Consequently, the activation energies must be considered as apparent values.

The apparent activation energy was determined from Fig. 10 at 0.7 of global true strain and with a c constant of 0.009 MPa^{-1} in the α + β and β field by an average value of the slope of the linear fit for each strain rate. The stress exponent was 3.5, similar value than those obtained for other metastable β and β-rich alloys [5,14]. The Q value obtained in the α + β region for Ti55531 was 275 kJ/mol, comparable with that obtained by Robertson et al. for Ti–10V–2Fe–3Al (294 kJ/mol) [16] but higher than that of the Ti-5-5-5-3 alloy (183 kJ/mol) [17]. The calculated apparent energy in the β region was 148 kJ/mol, which is similar to the value obtained for the self-diffusion of β phase (135–153 kJ/mol) [6–8] and for the deformation of some metastable beta and beta-rich alloys [5]. The linearity of the relation between flow stress and Z in Fig. 10b corroborates that the flow stress for all strain rates and temperatures in both fields follow the Eq. (1). Consequently, the constitutive equations at 0.7 of true strain can be written as:

$$\dot{\varepsilon} = 1.054 \times 10^{12}[\sinh(0.009\sigma_{0.7})]^{3.5} \exp\left(\frac{-275300}{RT}\right) \quad (5)$$

in the α + β field; and:

$$\dot{\varepsilon} = 6.18 \times 10^{5}[\sinh(0.009\sigma_{0.7})]^{3.5} \exp\left(\frac{-148000}{RT}\right) \quad (6)$$

in the β field.

Good correlation of the β subgrain size (δ_{ss}) and Z was observed below T_β (Fig. 11). The experimental relationship can be written as:

$$\delta_{ss} = 7 - 0.18 \ln(Z) \quad (7)$$

Thus, finer β subgrain results after deformation at lower temperature and higher strain rate (larger Z).

4. Discussion

Flow curves show an initial flow stress sharp peak followed by a drop in the stress at some deformation conditions. This phenomenon is related to a discontinuous yielding as was reported in previous works [5,30–33]. A pronounced discontinuous yielding was observed mainly at 0.1 s^{-1} and only in the β field at high strain

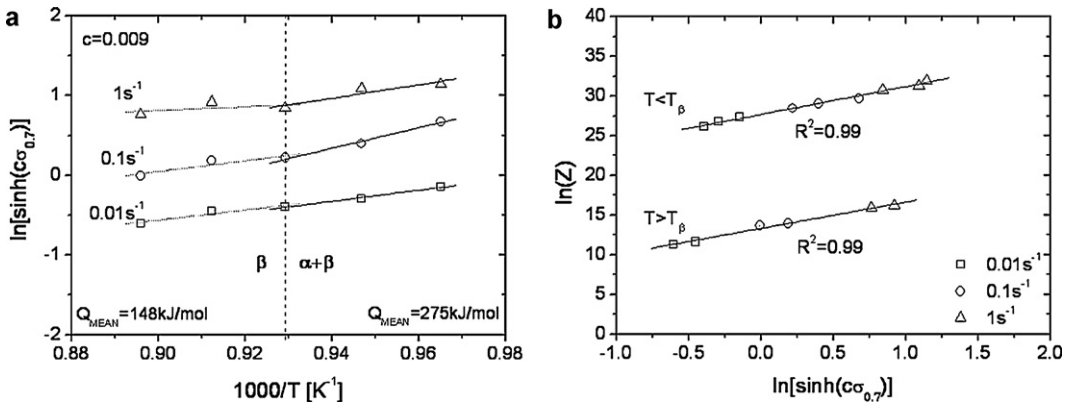

Fig. 10. (a) Determination of the activation energy from the slope of the linear regression in the α + β and β field for each strain rate at 0.7 of true strain. A mean value of *Q* was calculated from all the strain rates. (b) Zener–Hollomon parameter versus flow stress.

rates. For all the temperatures the yield drop values was highest at 0.1 s^{-1} strain rate [21]. This stress peak could be related to the presence of Fe and Cr in the β phase. Their small atomic radius and their high diffusivity compared with the other alloying elements can be related to the discontinuous yielding as described by the static theory. If this phenomenon is related to the dynamic theory, the higher content of the β-stabilizers in β phase, either in the near grain boundaries or within the grain, can intensify the solute–dislocation interaction, provoking a reduction of the mobile dislocation density. Consequently, new mobile dislocations must be generated upon deformation, with grain boundaries acting as sources, as was observed by Rack [30,33] and earlier by Margolin and Stanescu [34]. In general this behaviour is related to deformations in β single phase, although it was also reported for alloys deformed in the α + β field with more than 90% of β content [11,18].

4.1. Deformation in the α + β field

The restoration mechanisms after hot deformation below T_β (Figs. 6–8) occur mainly in the β phase. The linear correlation of the β subgrain size with the Zener Hollomon parameter (Fig. 10b) confirm that the main restoration of the β phase is dynamic recovery, as expected for a phase with low stacking fault energy [35]. The apparent energy value obtained in the α + β region is higher than the self-diffusion of the β phase and it should be related to the energy necessary to rotate, elongate and the α grains. Fig. 12 shows the boundary misorientation distribution of the β phase for different thermomechanical treatments at 763 °C. Table 1 summarizes the percentage of the high angle grain boundaries (%HAGB) and of the mean misorientation value (m_m). An increase of both %HAGB and m_m is observed with increasing deformation at 0.01 s^{-1}. The second phase (α) acts as a harder particle dispersed in the soft matrix pinning the dislocation movement and hence the β subgrains cannot grow beyond the α grains. This results in the formation of more HAGB by increasing the strain, suggesting geometric dynamic recrystallization (gDRX). The prior β grains became flattened with the strain and the grain boundaries took a serrated shape with a thickness of a few β subgrains producing pinching off of the grain boundary. It should be pointed out that the low sensi-

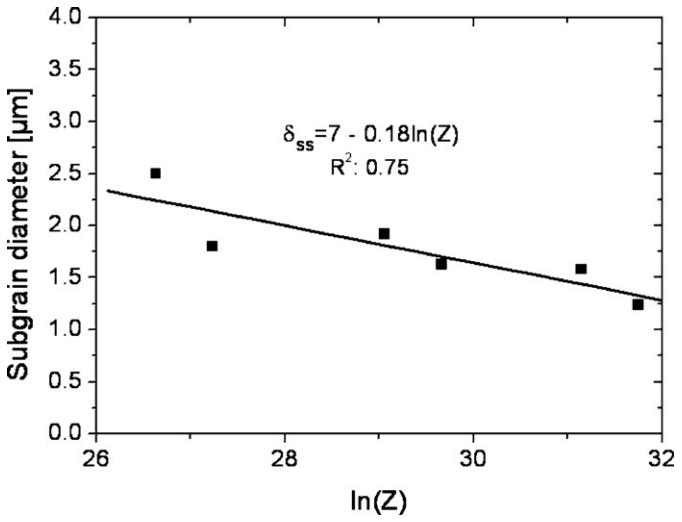

Fig. 11. Relationship between *Z* parameter and β subgrains diameter at 0.7 of strain.

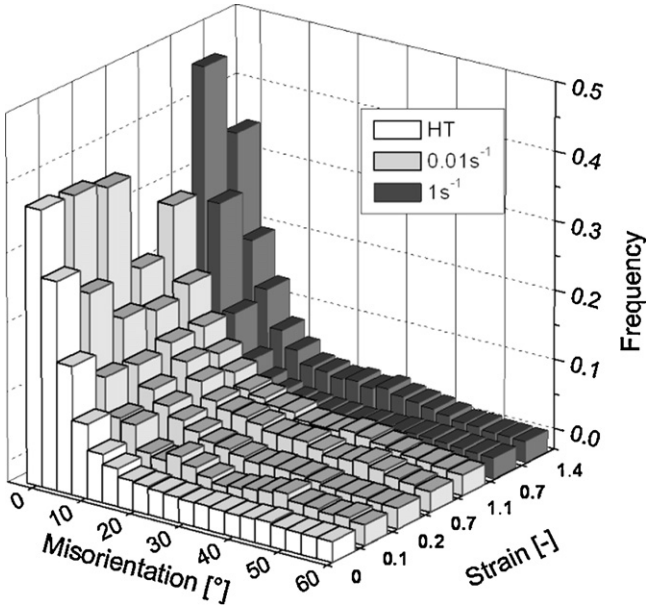

Fig. 12. Distribution of boundary misorientation in the β phase after heat treatment and deformation at 763 °C for different strains and strain rate.

Table 1
Mean misorientation values (m_m) and percentage of high angle grain boundary (%HAGB) in the beta phase of samples thermomechanical treated at 763 °C (corresponding to Fig. 12).

Strain rate	0	0.01s^{-1}				1s^{-1}	
Strain	0	0.1	0.2	0.7	1.1	0.7	1.4
m_m	10	12	13	17	15	9	13
%HAGB	13	22	28	41	34	11	27

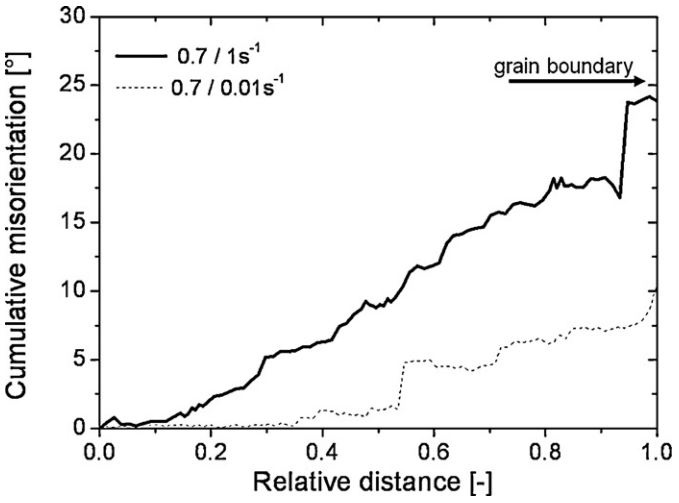

Fig. 13. Cumulative misorientations after deformations at 843 °C along the line (see arrows in Fig. 9) from the middle of the β grain to the grain boundary.

tivity of the misorientation angles obtained by EBSD compared to other methods [36] lead in an overestimation of the HAGB. Thus, the misorientation distributions should be used as comparative values between different conditions. The progressive lattice rotation of the β phase is the result of low dynamic recovery at high strain rates. This generates new HAGB near the prior β grain boundary. This effect was also observed by Furuhara et al. considering isothermal forging in α + β field with fine precipitated α grains dispersed in a larger volume of beta phase [11–13] and Montheillet et al. after torsion tests [14].

4.2. Deformation in the β field

In the β field, the calculated apparent activation energy fits well in the range of values obtained from the literature for self-diffusion in β-Ti supporting the theory that the dominant mechanism of restoration is dynamic recovery. Low strain rates promoted the formation of large subgrains. As occurred in the α + β field, prior grains became elongated and serrated grain boundaries formed. Pinching off can be observed in the case of very slow strain rates (large subgrains) and at elongated grain. On the other hand, at high strain rates, misorientations progressive increase within the beta grains towards the grain boundaries with subsequent formation of high angle grain boundaries. This reveals that dynamic recovery followed by continuous dynamic recrystallization by progressive lattice rotation is the predominant mechanism. Fig. 13 shows the cumulative misorientation within the beta grains in Fig. 9 (relative distance is 1 at the grain boundary). The cumulative misorientation is larger for grains deformed at high strain rates. These results agree with a similar behaviour reported in the beta-CEZ alloy [14], in single phase alloys with high stacking fault energy at larger deformations [37–39] and in AZ31 at high temperatures [40]. Timetal 555 was reported with dynamic recovery for temperatures near to the β transus and for specimens deformed above 1000 °C dynamic recrystallization was determined, although it was not determined if it was by discontinuous or continuous process [18].

5. Conclusions

Near beta titanium Ti55531 alloy has been studied during hot deformation near to the T_β. The flow stresses were correlated with the strain rate and the temperature (Zener Hollomon parameter) by the sinh equation. The use of the EBSD technique was necessary to determine the dynamic recovery and continuous dynamic recrystallization of the β phase as predominant mechanisms taking place during hot deformation. The conclusions can be summarized as follows:

- The main dynamic restoration mechanism is β dynamic recovery for all the deformation parameters.
- α + β field deformation occurs mainly by β-restoration with elongation and rotation of α grains perpendicular to the applied load.
- A progressive rotation of the lattice in the β phase occurs both in the α + β and β fields at high strain rates by increasing the strain. This rotation produces an increment of the cumulative misorientation distribution towards the prior β grain boundaries, generating new HAGB near the β prior grain by cDRX by lattice rotation.
- Low strain rates deformations are characterized by β-dynamic recovery in α + β as well as β fields at small strains. Pinching off of elongated prior grain boundaries take place at large strains producing new small grains by gDRX which locally takes place.

Acknowledgements

This work was carried out within the project “Modelling of microstructure and microstructure-dependent mechanical properties of near beta titanium alloys” sponsored by the Austrian Aeronautic programme “TAKE OFF” in cooperation with Böhler Schmiedetechnik GmbH & Co KG. The author would like to thank to Prof. D. Raabe and K. Angenendt from Max-Planck-Institut für Eisenforschung GmbH for the EBSD measurements and to USTEM at the Vienna Univ. of Technol. for provision of the EBSD and FEG-SEM facilities. Special thanks to Prof. H.P. Degischer for his priceless support in this work and to Prof. Alun Rhyswilliams for the correction of the manuscript.

References

[1] M. Ashby, H. Shercliff, D. Cebon, Materials: Engineering, Science, Processing and Design, Elsevier, Cambridge, 2007.
[2] G. Lütjering, J.C. Williams, Titanium, 1st ed., Springer, Berlin/Heidelberg, 2003.
[3] R.R. Boyer, R.D. Briggs, J. Mater. Eng. Perform. 14 (2005) 681–685.
[4] J.C. Fanning, R.R. Boyer, in: G. Luetjering, J. Albrecht (Eds.), Ti-2003: Sci. & Technol., Wiley-VCH, 2004, pp. 2643–2650.
[5] I. Weiss, S.L. Semiatin, Mater. Sci. Eng. A243 (1998) 46–65.
[6] N.E. Walsoe de Reca, C.M. Libanati, Acta Metall. 16 (1968) 1297–1305.
[7] D. Dyment, in: H. Kimura, O. Izumi (Eds.), Titanium ‘80: Sci. & Technol., TMS-AIME, 1980, pp. 519–528.
[8] J.F. Murdock, T.S. Lundy, E.E. Stansbury, Acta Metall. 12 (1964) 1033–1039.
[9] H.Z. Guo, Z.K. Yao, X.Y. Zhao, Y. Tan, in: G. Luetjering, J. Albrecht (Eds.), Ti-2003: Sci. & Technol., Wiley-VCH, 2004, pp. 603–609.
[10] V.V. Balasubrahmanyam, Y.V.R.K. Prasad, Mater. Sci. Technol. 17 (2001) 1222–1228.
[11] T. Furuhara, Y. Toji, T. Maki, in: G. Luetjering, J. Albrecht (Eds.), Ti-2003: Sci. & Technol., Wiley-VCH, 2004, pp. 1219–1226.
[12] T. Furuhara, B. Poorganji, H. Abe, T. Maki, J. Miner. Met. Mater. Soc. (JOM) 59 (2007) 64–67.
[13] T. Furuhara, H. Abe, B. Poorganji, T. Maki, in: M. Niinomi, S. Akiyama, M. Hagiwara, M. Ikeda, K. Maruyama (Eds.), Ti-2007: Sci. & Technol., JIM, 2007, pp. 913–920.
[14] F. Montheillet, D. Dajno, N. Come, E. Gautier, A. Simon, P. Audrerie, A.-M. Chaze, Ch. Levaillant, in: F.H. Froes, I. Caplan (Eds.), Titanium ‘92: Sci. & Technol., TMS, 1993, pp. 1347–1354.
[15] D.G. Robertson, H.B. McShane, Mater. Sci. Technol. 13 (1999) 575–583.
[16] D.G. Robertson, H.B. McShane, Mater. Sci. Technol. 14 (1998) 339–345.
[17] N.G. Jones, R.J. Dashwood, D. Dye, M. Jackson, Mater. Sci. Eng. A 490 (2008) 369–377.
[18] V. Venkatesh, M. Kamal, J. Fanning, in: M. Niinomi, S. Akiyama, M. Hagiwara, M. Ikeda, K. Maruyama (Eds.), Ti-2007: Sci. & Technol., JIM, 2007, pp. 503–506.
[19] V.V. Balasubrahmanyam, Y.V.R.K. Prasad, Mater. Sci. Eng. A 336 (2002) 150–158.
[20] I. Philippart, H.J. Rack, Mater. Sci. Eng. A 254 (1998) 253–267.
[21] F. Warchomicka, M. Stockinger, H.P. Degischer, in: M. Niinomi, S. Akiyama, M. Hagiwara, M. Ikeda, K. Maruyama (Eds.), Ti-2007: Sci. & Technol., JIM, 2007, pp. 511–514.
[22] Ti–5Al–5Mo–5V–3Cr–1Zr, Materials supplier receiving inspection report, VSMPO.
[23] C. Poletti, F. Warchomicka, H.P. Degischer, Mater. Sci. Eng. A 527 (2010) 1109–1116.

[24] F. Warchomicka, Ph.D. Thesis, Vienna University of Technology, Vienna, 2008.
[25] J.C. Fanning, J. Mater. Eng. Perform. 14 (2005) 788–791.
[26] I.S. Polkin, V.L. Rodionov, A.N. Stroshkov, T.V. Ishunkina, V.G. Kudryashov, O.S. Korobov, in: F.H. Froes, I. Caplan (Eds.), Titanium '92: Sci. & Technol., TMS, 1993, pp. 1569–1578.
[27] R. Boyer, G. Welsch, E.W. Collings, Materials Properties Handbook: Titanium Alloys, ASM International, Materials Park, USA, 1994.
[28] C.M. Sellars, W.J.McG. Tegart, Acta Metall. 14 (1966) 1136–1138.
[29] H.J. McQueen, N.D. Ryan, Mater. Sci. Eng. A 322 (2002) 43–63.
[30] I. Philippart, H.J. Rack, Mater. Sci. Eng. A 243 (1998) 196–200.
[31] M.N. Vijayshankar, S. Ankem, in: F.H. Froes, I. Caplan (Eds.), Titanium '92: Sci. & Technol., TMS, 1993, pp. 1733–1739.
[32] P. Wanjara, M. Jahazi, H. Monajati, S. Yue, J.-P. Immarigeon, Mater. Sci. Eng. A 396 (2005) 50–60.
[33] M. Long, H.J. Rack, in: P.A. Blenkinsop, W.J. Evans, H.M. Flower (Eds.), Titanium '95: Sci. & Technol., The Institute of Materials, London, 1996, pp. 316–323.
[34] H. Margolin, M.S. Stanescu, Acta Metall. 23 (1975) 1411–1418.
[35] F.J. Humphreys, M. Hantherly, Recrystallization and Related Annealing Phenomena, 2nd ed., Pergamon, New York, 2004.
[36] M. Cabibbo, W. Blum, E. Evangelista, M. Kassner, M. Meyers, Metall. Mater. Trans. A 39 (2008) 181–189.
[37] S. Gourdet, F. Montheillet, Mater. Sci. Eng. A 283 (2000) 274–288.
[38] H.J. McQueen, O. Knustad, N. Ryum, J.K. Solberg, Scripta Metall. 19 (1985) 73–78.
[39] P. Cizek, B.P. Wynne, Mater. Sci. Eng. A 230 (1997) 88–94.
[40] C. Poletti, F. Warchomicka, R. Okruch, H. Knoblich, Prakt. Met. 47 (2010) 517–529.